PAPER

Check for updates

Engineering earth-abundant copper(I) sensitizing centers in metal–organic frameworks for efficient photosynthesis†

Guang-Chen Guo, [ID] [a] Lihua Ma,*[ab] Xiao-Di Li,[a] Song Guo, [ID] *[a] Tong-Bu Lu [ID] [a] and Zhi-Ming Zhang [ID] *[a]

Rational construction of earth-abundant heterogeneous photocatalysts is of great importance for efficient and sustainable solar energy utilization. Herein, we have developed a series of earth-abundant MOF photocatalysts (Cu-1-MOF–Cu-5-MOF) by incorporating Cu(I) complexes with different steric functional groups, which represents an efficient strategy for regulating the sensitizing ability of MOFs by restricting the excited state configuration of Cu(I) sensitizing centers. Remarkably, Cu-5-MOF with strong steric functional groups can efficiently drive photocatalytic oxidative coupling of benzylamine with a yield of 90.2%, 11 times higher than that with Cu-1-MOF without steric functional groups (8.2%). Systematic investigations revealed that the introduction of strong steric functional groups (*e.g. sec*-butyl) into Cu based MOFs can enhance their visible-light absorption, photochemical stability and electron–hole separation efficiency, which contributed to facilitating the utilization of solar energy and interface electron/energy transfer for efficient photosynthesis. This work provides a new insight into rationally constructing earth-abundant and efficient MOF photocatalysts by engineering copper(I) sensitizing centers with steric functional groups at the molecular level.

[a]*Institute for New Energy Materials & Low Carbon Technologies, School of Material Science & Engineering, Tianjin University of Technology, Tianjin 300384, China. E-mail: malh987@hotmail.com; guosong@email.tjut.edu.cn; zmzhang@email.tjut.edu.cn*

[b]*School of Materials Science and Engineering, Harbin Institute of Technology, Harbin, 150001, China*

† Electronic supplementary information (ESI) available. See DOI: https://doi.org/10.1039/d3ta02142d
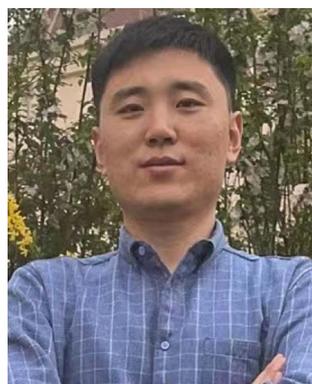
Dr Song Guo earned his PhD in Chemical Engineering and Technology in 2016 at the Dalian University of Technology (China). During the 2014–2015 year, he visited the University of Florida (USA) as a Joint PhD student. He is currently a Professor at the Institute for New Energy Materials and Low Carbon Technologies, Tianjin University of Technology. His current research interests focus on the development of artificial photosynthetic photosensitizers for solar energy conversion, including photochemical CO₂ reduction, water splitting and organic synthesis.

1 Introduction

Solar energy can be stored in carbohydrates *via* natural photosynthesis, which represents the largest scale matter and energy conversion process on the Earth. In this process, the magnesium porphyrin complex, as the active ingredient of chlorophyll in green leaves, is responsible for light absorption and electron transfer, largely determining the photosynthetic efficiency.[1] Therefore, the development of artificial photosensitizers (PSs) by mimicking the structure and function of chlorophyll represents a promising strategy to construct efficient photosynthetic systems. In this field, transition-metal-based photoactive complexes have been employed as light-harvesting PSs for solar energy conversion.[2–4] In particular, Ru- and Ir polypyridyl complexes can achieve long-lived metal-to-ligand charge transfer (MLCT) excited states, which have been widely applied to various photocatalytic reaction scenarios, such as organic synthesis,[5,6] H₂ evolution,[7–9] and CO₂ reduction.[10–12] However, these metal complex PSs in homogeneous systems were usually limited by their poor photochemical stability and excited state self-quenching and were difficult to recycle. Given that metal–organic frameworks (MOFs) as a class of structurally defined porous solid materials can provide an ideal molecular platform to stabilize solution-inaccessible metal active sites and rationally control the distance between metal sites,[13–19] typical [Ru(bpy)₃]²⁺ and [Ir(ppy)₂(bpy)]⁺ have been doped into MOFs for heterogeneous

photosynthesis.[20] Highly tunable MOFs can also hierarchically integrate Ru-/Ir complex PSs and catalysts to facilitate intra-framework energy and electron and mass transfers.[21–25] Sorts of catalysts, such as single metal sites and nanoclusters, have been embedded into Ru-/Ir complex sensitized MOFs for synergistic catalysis.[26–32] Despite significant progress, it's highly desirable but remains a great challenge to replace noble metal complexes with earth-abundant photoactive metal complexes in these crystalline MOF materials for efficient and sustainable photosynthesis.

Pioneered by the work of McMillin, Cu(I)–bis-phenanthrolines ([Cu(NN)$_2$]$^+$) with Cu(I) MLCT excited states have emerged as a most promising class of non-noble metal complexes for solar energy conversion.[33–35] In the ground state, the bis(diimine) Cu(I) structural motif with d^{10} configuration presented a pseudotetrahedral (D$_{2d}$) molecular geometry.[36] Upon light excitation, the resulting Cu(II) coordination center has a d^9 configuration *via* MLCT, which can trigger a Jahn–Teller (J–T) distortion owing to the unequal occupation of electrons in the degenerate 3d molecular orbitals.[37,38] After J–T distortion, a flattened conformation formed for the Cu(II) complex with a D_2 symmetry, which contributes to fully exposing the Cu(II) center to solvents and makes the Cu(II) center susceptible to nucleophilic attack from the donor solvents. Therefore, [Cu(NN)$_2$]$^+$ complexes usually presented a short-lived excited state and poor photo-chemical stability in Lewis basic solvents due to the formation of Cu(II)-solvent exciplexes. In the past half a century, attempts have been made to introduce steric functional groups in the 2- and 9- positions of the phenanthroline (**Phen**) ligands in [Cu(NN)$_2$]$^+$ for restricting their J–T distortion and improving their excited state properties.[39–42] However, to the best of our knowledge, the influence of excited state configuration on the sensitizing ability of Cu(I) complexes has never been explored in crystalline solid materials for heterogeneous photosynthesis.

In this work, for the first time, we have constructed a series of earth-abundant MOF photocatalysts *via* incorporation of Cu(I) complexes (**Cu-1-MOF**–**Cu-5-MOF**). The sensitizing ability of **Cu-MOFs** can be improved by systemically tuning the steric functional groups in the 2- and 9- positions of **Phen**. The catalytic activities for photo-oxidative coupling of benzylamine with these Cu(I)-based MOFs were in the order of **Cu-5-MOF** > **Cu-4-MOF** > **Cu-3-MOF** > **Cu-2-MOF** > **Cu-1-MOF**, well consistent with that of the steric resistance of their steric functional groups (Fig. 1). Remarkably, the conversion rates for benzylamine oxidative coupling can reach over 90.2% with **Cu-5-MOF** as the photocatalyst, representing the highest yield among all the **Cu-MOFs**. Systematic investigations reveal that the introduction of steric functional groups in **Phen** can improve the visible-light absorption, photochemical stability and electron–hole separation efficiency of photoactive MOFs, which contributed to facilitating the utilization of solar energy and interface electron/energy transfer for boosting photosynthesis. This work opened up a new avenue to develop efficient and earth-abundant MOF photocatalysts by restricting the excited state configuration of Cu(I) complexes.
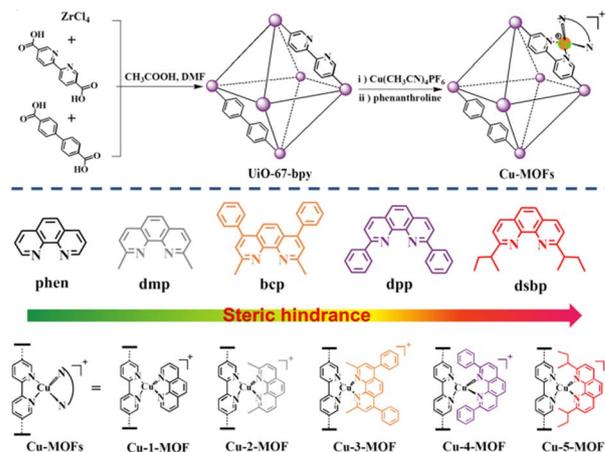

Fig. 1 Schematic view of the synthetic process (up) and the structures (down) of **Cu-MOFs**.

2 Experimental

2.1. Photocatalytic measurements

2.1.1 Aerobic oxidation coupling of benzylamine. 5.0 mg photocatalyst was added into the mixed solvent of 0.75 mL CH$_3$CN and 0.75 mL CH$_2$Cl$_2$ in a glass vial for ultrasonic dispersion. 0.02 mmol benzylamine was added into the above mixture, which was stirred in air upon irradiation with a 300 W Xe lamp (100 mW cm^{-2}, λ > 400 nm). The reaction process was monitored by TLC analysis. After the reaction is complete, the solvent is concentrated to dryness under reduced pressure. The conversion rate of crude products was determined by ^{1}H NMR. For the recycling experiments, the photocatalyst was collected by centrifugation and washed with CH$_2$Cl$_2$. After drying in a vacuum oven at 50 °C for 3 h, the sample powder was used for the next round of photocatalysis.

2.2. Synthesis of MOFs

2.2.1 Synthesis of UiO-67-bpy. ZrCl$_4$ (10.0 mg, 0.042 mmol), 4,4′-biphenyldicarboxylic acid (H$_2$bdc, 6.0 mg, 0.025 mmol), 2,2′-bipyridine-5,5′-dicarboxylic acid (H$_2$bpydc, 4.0 mg, 0.016 mmol) and glacial acetic acid (83 μL) were mixed in 1.5 mL DMF. After being sealed in a vial, the mixture was placed in an oven. The temperature was kept at 100 °C for 24 h. After cooling down to room temperature, the resulting precipitate was collected by centrifugation, washed with DMF/CH$_3$OH and dried under vacuum at 100 °C to afford 12.5 mg UiO-67-bpy with a yield of ~84.2%.

2.2.2 Synthesis of Cu-MOFs. UiO-67-bpy (50.0 mg) was dispersed in 10 mL CH$_3$CN and transferred into a dried 50 mL three-neck round-bottom flask. Cu(CH$_3$CN)$_4$PF$_6$ (93.2 mg, 0.25 mmol) in 10 mL CH$_2$Cl$_2$ was added to the above flask and the mixture was stirred for 24 h under argon. After the reaction was complete, the solid was collected by centrifugation and washed with CH$_2$Cl$_2$ several times to remove excess Cu salt. The resulting solid and phenanthroline ligands (0.10 mmol) were added into the mixed solvent of 2 mL CH$_2$Cl$_2$ and 1 mL

CH₃CN, which was stirred for 24 h. After the reaction was complete, the product was collected by centrifugation, washing with CH_2Cl_2 and drying under vacuum at 50 °C to afford the **Cu-MOFs**.

3   Results and discussion

3.1.   Synthesis and characterization

A series of Cu(ɪ)-based MOF photocatalysts (**Cu-MOFs**) were successfully synthesized through a modular step-by-step assembly strategy (Fig. 1). Using UiO-67-bpy as a molecular platform, $Cu(CH_3CN)_4PF_6$ was first coordinated to the diimide sites of the bpy ligands in MOFs, and then **Phen** with different steric functional groups could be coordinated to the Cu(ɪ) sites to afford the Cu(ɪ) complex sensitized MOFs (**Cu-1-MOF–Cu-5-MOF**) (Fig. S1†). Cu(ɪ)-based MOFs were fully characterized using the powder X-ray diffraction pattern (PXRD), X-ray photoelectron spectroscopy (XPS), a scanning electron microscope (SEM) and a transmission electron microscope (TEM) (Fig. S2–S5†). As shown in Fig. S2,† the characteristic peaks of PXRD for UiO-67-bpy were well consistent with that of the simulated PXRD pattern of UiO-67, indicating the correct structure and good phase purity of UiO-67-bpy. The PXRD patterns of **Cu-MOFs** were similar to those of UiO-67-bpy, confirming the well maintained structure and crystallinity before and after incorporating Cu(ɪ) complexes. As shown in Fig. S4,† the two main peaks at 932.2 and 952.0 eV correspond to Cu $2p_{1/2}$ and Cu $2p_{3/2}$, respectively, which could be attributed to Cu(ɪ).

SEM and TEM analyses revealed that **Cu-5-MOF** exhibited a regular uniform octahedral morphology with a size of *ca.* 400 nm (Fig. S5†).

Besides, elemental mapping images showed the even distribution of Zr, Cu, C, N and O elements in the **Cu-5-MOF** skeleton, further supporting that Cu(ɪ) complexes were successfully introduced into UiO-67-bpy (Fig. 2). Inductively coupled plasma mass spectrometry (ICP-MS) analysis manifested that these different **Cu-MOFs** exhibited a similar Cu content (Table S1†), precluding the influence of Cu content differences in different MOFs on their catalytic performance.
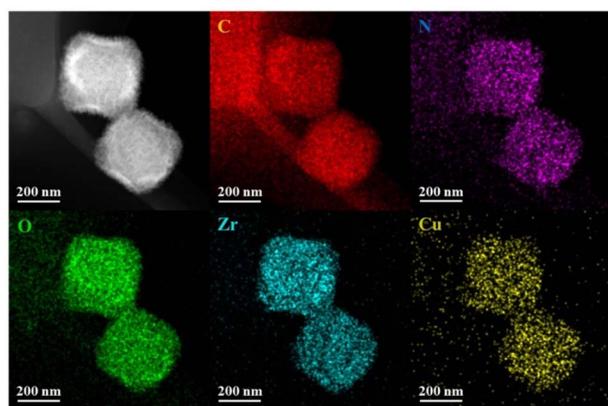

Fig. 2   High angle annular dark field scanning transmission electron microscopy and elemental mapping images of **Cu-5-MOF**.

3.2.   Photophysical and electrochemical characterization

Visible light harvesting ability and photoelectrochemical properties of **Cu-MOFs** were systematically investigated using steady/transient spectra and photocurrent/electro-chemical impedance spectroscopy (Fig. 3). As shown in Fig. 3a, the absorption of UiO-67-bpy was mainly limited in the ultraviolet region, which was harmful to the utilization of solar energy. After the introduction of Cu(ɪ) complexes, the absorption of UiO-MOFs can be expanded to the visible light region. **Cu-5-MOF** exhibited a visible light absorption peak at around 450 nm, similar to that of **Cu-2-MOF**. This indicated that 2,9-di(*sec*-butyl)**Phen** and 2,9-dimethyl**Phen** modified Cu-based MOFs possessed a similar electronic configuration in the ground state. The absorption of **Cu-3-MOF** extended to 490 nm as compared with that of **Cu-2-MOF**, which could be attributed to an extended conjugated system of ligands due to the introduction of phenyl at the 4 and 7-positions of **Phen**. Besides, **Cu-4-MOF** presented a much broader visible absorption than other **Cu-MOFs**, well consistent with the absorbing feature of the reported PS $[Cu(\mathbf{dpp})_2]^+$ (**dpp** = 2,9-diphenylphenanthroline).[43] Both the emission and photoluminescence lifetimes of UiO-67-bpy significantly quenched after introducing Cu(ɪ) complexes (Fig. 3b and S6, S7†). This could be ascribed to the transformation from the singlet state of UiO-67-bpy into the triplet state of the Cu(ɪ) complex.[42,44] The photocurrent intensity was in the order of **Cu-5-MOF** > **Cu-4-MOF** > **Cu-3-MOF** > **Cu-2-MOF** > **Cu-1-MOF**, well consistent with that of the steric resistance of their steric functional groups (Fig. 3c). This result revealed that Cu(ɪ) complexes with large steric functional groups contributed to facilitating photogenerated electron–hole separation of photoactive MOFs. Notably, **Cu-5-MOF** exhibited the most efficient electron–hole separation among **Cu-MOFs** due to the restricted J–T distortion of *sec*-butyl steric functional groups to reduce the excited state
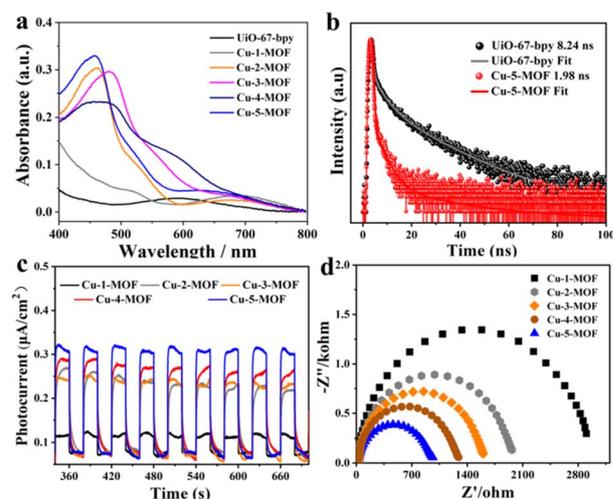

Fig. 3   (a) UV-vis absorption spectra of UiO-67-bpy and **Cu-MOFs**, (b) Photoluminescence lifetimes of UiO-67-bpy and **Cu-5-MOF**, and (c) and (d) photocurrent response and Nyquist plots of the electrochemical impedance spectra (EIS) of **Cu-MOFs** under 300 W Xe lamp irradiation.

loss *via* non-radiation transition.[40] This viewpoint was further supported by their electrochemical impedance spectra (EIS), where their EIS radii were in the order of **Cu-5-MOF** < **Cu-4-MOF** < **Cu-3-MOF** < **Cu-2-MOF** < **Cu-1-MOF** (Fig. 3d). Furthermore, the energy level diagram of the highest occupied molecular orbital (HOMO) and lowest unoccupied molecular orbital (LUMO) for UiO-67-bpy and **Cu-MOFs** can be estimated by Mott–Schottky (MS) measurements and Tauc plot analysis (Fig. S8 and S9†). The calculated LUMO level of **Cu-MOFs** was determined to be -0.60 V $-$ -0.85 V, more negative than the reduction potential from O_2 to superoxide radicals ($E(O_2/O_2^{\bullet-}) = -0.33$ V *vs.* NHE) (Fig. S10†), indicating that the electron transfer from the LUMO of photoactive **Cu-MOFs** to O_2 was thermodynamically feasible. As a result, **Cu-5-MOF** with large steric functional groups exhibited favorable visible absorption and efficient electron–hole separation, highlighting its great potential for solar energy conversion.

3.3. Photocatalytic oxidation reactions

Imines, as active intermediates, played an important role in the synthesis of dyes, drugs and agricultural chemicals. Photocatalytic oxidative coupling of amines represented a mild, clean and efficient approach for the synthesis of imines.[45] Here we examined the sensitizing ability of **Cu-MOFs** by photo-oxidative coupling of benzylamines. As shown in Fig. 4a, upon irradiation with visible light, the yield of product **2a** (*N*-benzylidene-benzylamine) was in the order of **Cu-5-MOF** > **Cu-4-MOF** > **Cu-3-MOF** > **Cu-2-MOF** > **Cu-1-MOF** > UiO-67-bpy (Table S2†). Remarkably, the yield of **2a** with the **Cu-5-MOF** photocatalyst can reach 90.2% within 1 hour, 11 times higher than that with **Cu-1-MOF** (8.2%). The poor catalytic performance of **Cu-1-MOF** could be mainly ascribed to its excitation energy loss by J–T distortion due to no steric functional groups in **Phen** ligands. There was almost no product formed in the absence of oxygen,

visible light or photocatalyst, indicating that these factors were essential for efficient photosynthesis (Fig. S11†).

Remarkably, there was no significant loss of catalytic activity for **Cu-5-MOF** after five consecutive recycles (Fig. 4b), indicating its excellent catalytic stability. This viewpoint was further supported by the results of PXRD and SEM, where the structure, crystallinity and octahedral configuration of **Cu-5-MOF** were well maintained after the photocatalytic reaction (Fig. S12 and S13†). As compared with **Cu-5-MOF**, **Cu-1-MOF** and **Cu-3-MOF** presented a poor photochemical stability (Fig. S14†). In addition, benzylamine derivatives with different substituents could be effectively transformed into imines with **Cu-5-MOF** photocatalysts under visible light. As shown in Table S3,† the conversion of all the substrates can reach over 74% within 1.5 h, confirming a broad substrate tolerance for the **Cu-5-MOF** photocatalyst.

In order to unveil the superior catalytic performance of **Cu-5-MOF**, a series of control experiments were carried out and electron spin resonance (ESR) spectra were recorded to comprehensively study its catalytic mechanism (Fig. 4c, d and Table S4†). *p*-Benzoquinone (BQ), NaN_3 and isopropanol (IPA) were used as $O_2^{\bullet-}$, $^1O_2$ and $^{\bullet}OH$ scavengers, respectively. The conversion of benzylamine significantly decreased upon the addition of BQ and NaN_3, which preliminarily confirmed that both $^1O_2$ and $O_2^{\bullet-}$ were reactive oxygen species (ROS) for efficient photooxidation. After adding IPA, the catalytic yield was well maintained, excluding the possibility of $^{\bullet}OH$ participating in the reaction. As shown in Table S4† the conversion rate of benzylamine decreased in the presence of hydroquinone (HQ), KI and $AgNO_3$ as free radicals, holes and electron scavengers, respectively, further supporting that the catalytic process was mediated by the electron transfer pathway. To further discern ROS in the catalytic process, ESR experiments were performed with 4-oxo-TMP and 5, 5-dimethyl-1-pyrroline *N*-oxide (DMPO) as $^1O_2$ and $O_2^{\bullet-}$ trapping agents, respectively (Fig. 4c and d). Upon light irradiation, the characteristic signals of the complexes $^1O_2$-4-oxo-TMP and $O_2^{\bullet-}$-DMPO were observed, which almost completely disappeared after the addition of benzylamine. This further verified that both $^1O_2$ and $O_2^{\bullet-}$ indeed participated in the photosynthetic reaction. As shown in Fig. S15,† a characteristic absorption band between 450–600 nm was observed for reaction solution in the presence of DPD (*N*,*N*-diethyl-*p*-phenylenediamine)/POD (horseradish peroxidase), confirming the production of H_2O_2 in the photocatalysis process of benzylamine oxidative coupling.

Based on the above systematic investigations, the catalytic mechanism for the photocatalytic aerobic coupling of benzylamine was proposed as follows (Fig. 5): upon visible light irradiation, the triplet state of Cu(I) complexes in MOFs was populated by a series of intramolecular photophysical processes, which can facilitate photogenerated electron–hole (e^-–h^+) separation of MOFs. Subsequently, the photogenerated electrons and holes can transfer to O_2 and benzylamine to generate $O_2^{\bullet-}$ and $PhCH_2NH_2^{\bullet+}$, respectively. $PhCH_2NH_2^{\bullet+}$ can react with $O_2^{\bullet-}$ to generate $PhCH=NH$. In the meantime, the excitation energy of the Cu(I) complex can be transferred to O_2 *via* the Dexter mechanism to afford $^1O_2$, which can react with
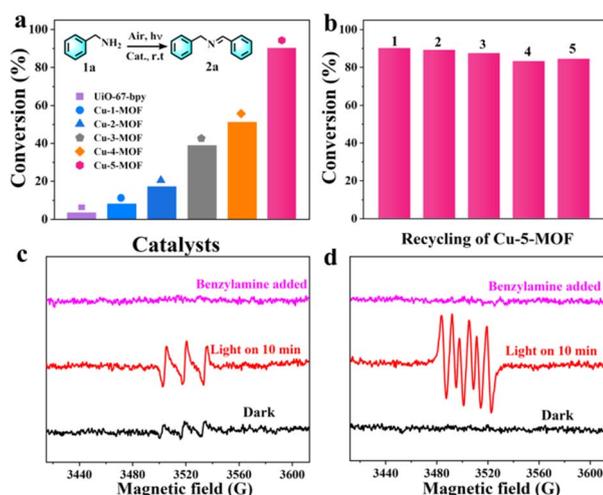

Fig. 4 (a) Catalytic activities of UiO-67-bpy and **Cu-MOFs** for aerobic photocatalytic oxidative coupling of benzylamine. (b) Recycling experiments with **Cu-5-MOF**. (c) and (d) ESR spectra of **Cu-5-MOF** in the presence of 4-oxo-TMP in CH_3CN and DMPO in DMSO.
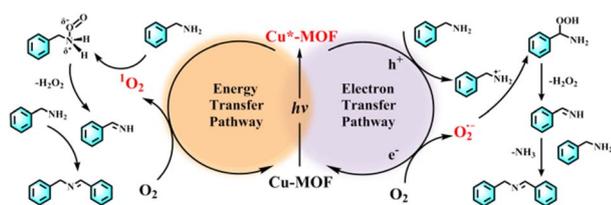
This journal is © The Royal Society of Chemistry 2023

J. Mater. Chem. A, 2023, **11**, 14052–14057 | **14055**

Fig. 5 The proposed catalytic mechanism of the aerobic oxidative coupling of benzylamine with O_2 using **Cu-5-MOF** as the photocatalyst.

benzylamine to generate PhCH=NH. Ultimately, PhCH=NH coupled with benzylamine to produce *N*-benzylidenebenzylamine. As a result, the catalytic performance of **Cu-MOFs** highly depended on their visible light harvesting ability, electron–hole separation ability and interface energy/electron efficiency.

2-Chloroethyl ethyl sulfide (CEES) as a chemical warfare agent simulant can be transformed into nontoxic 2-chloroethyl ethyl sulfoxide (CEESO) by the photochemical strategy.[46–48] In order to verify the universality of the regulation strategy of **Cu-MOF** sensitizing ability by restricting their excited state configuration, these **Cu-MOFs** were applied to photo-oxidative degradation of CEES to produce CEESO. Remarkably, the catalytic yield of CEESO with **Cu-5-MOF** can reach 100% under visible light irradiation, significantly higher than that with **Cu-1-MOF** and **Cu-2-MOF** (Table S5†). This result revealed that Cu(I) complexes with strong steric functional groups in MOFs exhibited a much stronger sensitizing ability than that with weak or no steric functional groups in MOFs. This could be ascribed to that Cu(I) complexes with strong steric functional groups in MOFs can restrict its J–T distortion to reduce the excitation energy loss. Control experiments and ESR spectra confirmed that both $^1O_2$ and $O_2^{\cdot-}$ were ROS in the catalytic process (Table S6, Fig. S16 and S17†). As shown in Fig. S18,† the excited **Cu-5-MOF** sensitized O_2 to produce $^1O_2$ and $O_2^{\cdot-}$ by the energy/electron transfer process, which can further oxidize the substrates to CEESO.

4 Conclusions

In summary, for the first time, we constructed a series of earth-abundant and efficient MOF photocatalysts by incorporating Cu(I) complexes with different steric functional groups. The influence of excited state configuration of Cu(I) complexes on MOF sensitizing ability was first explored by systemically varying steric functional groups. Remarkably, the conversion rates for benzylamine oxidative coupling can reach over 90.2% with **Cu-5-MOF** as the photocatalyst, 11 and 5.2 times higher than that with **Cu-1-MOF** (8.2%) and **Cu-2-MOF** (17.2%), respectively. In addition, the **Cu-5-MOF** photocatalyst can be recycled and reused for over 5 times without the obvious activity loss, representing a robust photochemical stability, much superior to that of **Cu-1-MOF** and **Cu-3-MOF**. **Cu-5-MOF** with large steric functional groups in **Phen** can increase torsional resistance and reduce the excitation loss of MOF photocatalysts, resulting in its advantages in strong visible light absorption,

efficient electron–hole separation and good photochemical stability, which greatly contributed to boosting photosynthesis. This work opens a new horizon for the development of highly efficient and earth-abundant MOF photocatalysts by restricting the excited state configuration at the molecular level.

Author contributions

S. G. conceived and designed the project, G. C. G. and X. D. L. performed the experiments, G. C. G., L. H. M., X. D. L., S. G., T. B. L. and Z. M. Z. analyzed the data and wrote the article.

Conflicts of interest

There are no conflicts to declare.

Acknowledgements

References

1 T. Mirkovic, E. E. Ostroumov, J. M. Anna, R. van Grondelle, Govindjee and G. D. Scholes, *Chem. Rev.*, 2017, **117**, 249–293.
2 D. N. Tritton, F.-K. Tang, G. B. Bodedla, F.-W. Lee, C.-S. Kwan, K. C.-F. Leung, X. Zhu and W.-Y. Wong, *Coord. Chem. Rev.*, 2022, **459**, 214390.
3 Y. J. Yuan, Z. T. Yu, D. Q. Chen and Z. G. Zou, *Chem. Soc. Rev.*, 2017, **46**, 603–631.
4 J. Zhao, W. Wu, J. Sun and S. Guo, *Chem. Soc. Rev.*, 2013, **42**, 5323–5351.
5 Q. Liu and L.-Z. Wu, *Natl. Sci. Rev.*, 2017, **4**, 359–380.
6 C. K. Prier, D. A. Rankic and D. W. MacMillan, *Chem. Rev.*, 2013, **113**, 5322–5363.
7 M. Wang, K. Han, S. Zhang and L. Sun, *Coord. Chem. Rev.*, 2015, **287**, 1–14.
8 P. Wang, S. Guo, H. J. Wang, K. K. Chen, N. Zhang, Z. M. Zhang and T. B. Lu, *Nat. Commun.*, 2019, **10**, 3155.
9 S. Guo, K.-K. Chen, R. Dong, Z.-M. Zhang, J. Zhao and T.-B. Lu, *ACS Catal.*, 2018, **8**, 8659–8670.
10 Y. Kuramochi, O. Ishitani and H. Ishida, *Coord. Chem. Rev.*, 2018, **373**, 333–356.
11 Y.-H. Luo, L.-Z. Dong, J. Liu, S.-L. Li and Y.-Q. Lan, *Coord. Chem. Rev.*, 2019, **390**, 86–126.
12 Y. Hu, F. Zhan, Q. Wang, Y. Sun, C. Yu, X. Zhao, H. Wang, R. Long, G. Zhang, C. Gao, W. Zhang, J. Jiang, Y. Tao and Y. Xiong, *J. Am. Chem. Soc.*, 2020, **142**, 5618–5626.
13 K. Sun, Y. Qian and H. L. Jiang, *Angew. Chem., Int. Ed.*, 2023, **62**, e202217565.
14 B. Li, M. Chrzanowski, Y. Zhang and S. Ma, *Coord. Chem. Rev.*, 2016, **307**, 106–129.
15 C. D. Wu and M. Zhao, *Adv. Mater.*, 2017, **29**, 1605446.
16 J. Liu, L. Chen, H. Cui, J. Zhang, L. Zhang and C. Y. Su, *Chem. Soc. Rev.*, 2014, **43**, 6011–6061.
17 L. Zeng, X. Guo, C. He and C. Duan, *ACS Catal.*, 2016, **6**, 7935–7947.

14056 | *J. Mater. Chem. A*, 2023, **11**, 14052–14057

This journal is © The Royal Society of Chemistry 2023

18 A. Kirchon, L. Feng, H. F. Drake, E. A. Joseph and H. C. Zhou, *Chem. Soc. Rev.*, 2018, **47**, 8611–8638.

19 Y. Bai, Y. Dou, L. H. Xie, W. Rutledge, J. R. Li and H. C. Zhou, *Chem. Soc. Rev.*, 2016, **45**, 2327–2367.

20 C. Wang, Z. Xie, K. E. deKrafft and W. Lin, *J. Am. Chem. Soc.*, 2011, **133**, 13445–13454.

21 C.-C. Hou, T.-T. Li, S. Cao, Y. Chen and W.-F. Fu, *J. Mater. Chem. A*, 2015, **3**, 10386–10394.

22 G. Lan, Z. Li, S. S. Veroneau, Y. Y. Zhu, Z. Xu, C. Wang and W. Lin, *J. Am. Chem. Soc.*, 2018, **140**, 12369–12373.

23 P. M. Stanley, J. Haimerl, C. Thomas, A. Urstoeger, M. Schuster, N. B. Shustova, A. Casini, B. Rieger, J. Warnan and R. A. Fischer, *Angew. Chem., Int. Ed.*, 2021, **60**, 17854–17860.

24 P. M. Stanley, C. Thomas, E. Thyrhaug, A. Urstoeger, M. Schuster, J. Hauer, B. Rieger, J. Warnan and R. A. Fischer, *ACS Catal.*, 2021, **11**, 871–882.

25 D. Kim, D. R. Whang and S. Y. Park, *J. Am. Chem. Soc.*, 2016, **138**, 8698–8701.

26 Z.-H. Yan, B. Ma, S.-R. Li, J. Liu, R. Chen, M.-H. Du, S. Jin, G.-L. Zhuang, L.-S. Long, X.-J. Kong and L.-S. Zheng, *Sci. Bull.*, 2019, **64**, 976–985.

27 T. C. Zhuo, Y. Song, G. L. Zhuang, L. P. Chang, S. Yao, W. Zhang, Y. Wang, P. Wang, W. Lin, T. B. Lu and Z. M. Zhang, *J. Am. Chem. Soc.*, 2021, **143**, 6114–6122.

28 S. Guo, L. H. Kong, P. Wang, S. Yao, T. B. Lu and Z. M. Zhang, *Angew. Chem., Int. Ed.*, 2022, **61**, e202206193.

29 C. Wang, K. E. deKrafft and W. Lin, *J. Am. Chem. Soc.*, 2012, **134**, 7211–7214.

30 W. Huang, X. Wang, W. Zhang, S. Zhang, Y. Tian, Z. Chen, W. Fang and J. Ma, *Appl. Catal., B*, 2020, **273**, 119087.

31 W. Wang, X.-W. Song, Z. Hong, B. Li, Y. Si, C. Ji, K. Su, Y. Tan, Z. Ju, Y. Huang, C.-N. Chen and D. Yuan, *Appl. Catal., B*, 2019, **258**, 117979.

32 W.-M. Liao, J.-H. Zhang, Z. Wang, S.-Y. Yin, M. Pan, H.-P. Wang and C.-Y. Su, *J. Mater. Chem. A*, 2018, **6**, 11337–11345.

33 R. M. Everly, R. Ziessel, J. Suffert and D. R. McMillin, *Inorg. Chem.*, 1991, **30**, 559–561.

34 M. Iwamura, S. Takeuchi and T. Tahara, *Acc. Chem. Res.*, 2015, **48**, 782–791.

35 D. G. Cuttell, S. M. Kuang, P. E. Fanwick, D. R. McMillin and R. A. Walton, *J. Am. Chem. Soc.*, 2002, **124**, 6–7.

36 N. A. Gothard, M. W. Mara, J. Huang, J. M. Szarko, B. Rolczynski, J. V. Lockard and L. X. Chen, *J. Phys. Chem. A*, 2012, **116**, 1984–1992.

37 M. Iwamura, S. Takeuchi and T. Tahara, *J. Am. Chem. Soc.*, 2007, **129**, 5248–5256.

38 S. Garakyaraghi, E. O. Danilov, C. E. McCusker and F. N. Castellano, *J. Phys. Chem. A*, 2015, **119**, 3181–3193.

39 M. Iwamura, S. Takeuchi and T. Tahara, *Phys. Chem. Chem. Phys.*, 2014, **16**, 4143–4154.

40 C. T. Cunningham, K. L. Cunningham, J. F. Michalec and D. R. McMillin, *Inorg. Chem.*, 1999, **38**, 4388–4392.

41 M. C. Rosko, K. A. Wells, C. E. Hauke and F. N. Castellano, *Inorg. Chem.*, 2021, **60**, 8394–8403.

42 K. K. Chen, S. Guo, H. Liu, X. Li, Z. M. Zhang and T. B. Lu, *Angew. Chem., Int. Ed.*, 2020, **59**, 12951–12957.

43 M. Ruthkosky, F. N. Castellano and G. J. Meyer, *Inorg. Chem.*, 1996, **35**, 6406–6412.

44 M. W. Mara, D. N. Bowman, O. Buyukcakir, M. L. Shelby, K. Haldrup, J. Huang, M. R. Harpham, A. B. Stickrath, X. Zhang, J. F. Stoddart, A. Coskun, E. Jakubikova and L. X. Chen, *J. Am. Chem. Soc.*, 2015, **137**, 9670–9684.

45 C. Xu, H. Liu, D. Li, J. H. Su and H. L. Jiang, *Chem. Sci.*, 2018, **9**, 3152–3158.

46 H. Wang, G. W. Wagner, A. X. Lu, D. L. Nguyen, J. H. Buchanan, P. M. McNutt and C. J. Karwacki, *ACS Appl. Mater. Interfaces*, 2018, **10**, 18771–18777.

47 A. Atilgan, M. M. Cetin, J. Yu, Y. Beldjoudi, J. Liu, C. L. Stern, F. M. Cetin, T. Islamoglu, O. K. Farha, P. Deria, J. F. Stoddart and J. T. Hupp, *J. Am. Chem. Soc.*, 2020, **142**, 18554–18564.

48 H. Wang, S. Jiang, S. Chen, D. Li, X. Zhang, W. Shao, X. Sun, J. Xie, Z. Zhao, Q. Zhang, Y. Tian and Y. Xie, *Adv. Mater.*, 2016, **28**, 6940–6945.

This journal is © The Royal Society of Chemistry 2023

J. Mater. Chem. A, 2023, **11**, 14052–14057 | **14057**